Research Article

Annaclaudia Burrelli, Paolo Moretti, Yuri Gerelli*, Maria Grazia Ortore*

Effects of model membranes on lysozyme amyloid aggregation

https://doi.org/10.1515/bmc-2022-0034
received April 30, 2023; accepted July 13, 2023

Abstract: The study of the interaction between lipid membranes and amyloidogenic peptides is a turning point for understanding the processes involving the cytotoxicity of peptides involved in neurodegenerative diseases. In this work, we perform an experimental study of model membrane–lysozyme interaction to understand how the formation of amyloid fibrils can be affected by the presence of polar and zwitterionic phospholipid molecules (1-palmitoyl-2-oleoyl-sn-glycero-3-phosphocholine [POPC] and 1-palmitoyl-2-oleoyl-sn-glycero-3-phosphoglycerol [POPG]). The study was conducted above and below the critical micellar concentration (CMC) using dynamic light scattering (DLS), atomic force microscopy (AFM), UV–Vis spectrophotometry, and the quartz crystal microbalance (QCM). Our results show that the presence of phospholipids appears to be a factor favoring the formation of amyloid aggregates. Spectrophotometric and DLS data revealed that the quantity of β-structure increases in the presence of POPG and POPC at different concentrations. The presence of POPG and POPC increases the speed of the nucleation process, without altering the overall structures of the fibrillar final products.

Keywords: amyloid, membrane, DLS, AFM, QCM

Introduction

The misfolding and aggregation of otherwise functional proteins are known to be correlated with several neurodegenerative disorders, like Alzheimer's and Parkinson's diseases, as well as systemic amyloidoses [1]. Fundamental research projects focused on the fact that the protein fibrils found in association with these pathologies share common properties, such as a core rich in β-sheet structures adopting a characteristic cross-β topology and tensile strength [2,3]. These features are not necessarily linked to a precise pathology but have been recognized as common in several proteins able to form amyloid fibrils in stress conditions (extreme pHs, high temperature, etc.) [4].

Although the structural similarity between the mature amyloid aggregates [5–7] could suggest the existence of some generic mechanism of toxicity, it was suggested, in the last decades, that the oligomeric species, precursors of amyloid fibrils, were the most cytotoxic aggregates [8–12]. The existence of amyloid plaques and tangles in the brain was considered a common finding in Alzheimer's pathology; however, results from the "Nun study" indicated that neurofibrillary tangles located in regions of the brain outside the neocortex and hippocampus may have less of an effect than plaques located within those areas [13], suggesting the possibility of compensatory biological mechanisms with respect to fibrils neurotoxicity, and/or other neurotoxic patterns [14].

The investigation of the interaction between amyloidogenic peptides and cell membranes is key to understanding the processes involved in their cytotoxicity. In the last decades, researchers have started to compare the cytotoxic processes induced by the same molecule in different states of aggregation (native, small oligomers, and large fibrils), without finding so far any general behavior. In some cases, the formation of large aggregates has been proposed as a *self-defense* process to hinder the interaction between fibrils and cell membranes and, in turn, prevent cellular damage. On the contrary, pronounced cytotoxicity was found when the same molecular species were forming small oligomers, i.e., at the onset of aggregation. For example, in the case of the

*** Corresponding author: Yuri Gerelli,** Department of Life and Environmental Sciences, Marche Polytechnic University, Ancona, Italy; CNR Institute for Complex Systems, Piazzale Aldo Moro 5, 00185 Roma, Italy; Department of Physics, Sapienza University of Rome, Piazzale Aldo Moro 5, 00185 Roma, Italy, e-mail: yuri.gerelli@cnr.it
*** Corresponding author: Maria Grazia Ortore,** Department of Life and Environmental Sciences, Marche Polytechnic University, Ancona, Italy, e-mail: m.g.ortore@univpm.it
Annaclaudia Burrelli, Paolo Moretti: Department of Life and Environmental Sciences, Marche Polytechnic University, Ancona, Italy

human islet amyloid polypeptide (hIAPP), a peptide involved in type 2 Diabetes Mellitus, it was shown that small hIAPP oligomers promoted lipid depletion from cell membrane mimics while amyloidogenic aggregation inhibited the process of membrane permeation [15]. In this framework, the relationship between the protein aggregation pathway leading to the formation of amyloid fibrils and the presence of other biomolecules, such as lipids, that the proteins may encounter in body fluids has been investigated but is not yet fully understood. Indeed, the presence of lipid molecules in and around amyloid fibrils was confirmed by different studies [16–18] and excluded by others [19]. Furthermore, it is not yet clear how the presence of lipids in solution can modify not just fibrils structure but even their nucleation and growth. Another debated topic is the influence of the aggregation state of the lipid molecules on the formation of fibrils. Lindberg et al. [20] showed that the presence of lipid vesicles composed of zwitterionic molecules accelerates the fibril growth rate for Aβ(1-42). Moreover, they found that lipid vesicles have no effect on primary nucleation, while they increase secondary nucleation at the surface of existing fibrils. More recently, several computational and experimental studies [15,21,22] pointed out a possible lipid-chaperone effect, in which free lipids can interact with peptide monomers and small oligomers forming protein–lipid complexes with a larger affinity for cell membranes, i.e., with different cytotoxicity. It is clear that although several studies have been performed on the effects of model membranes of protein amyloid aggregation, the results are not always coherent. Further efforts are needed to clarify the influence of lipid components, both for their intrinsic properties (charge, chemical features, etc.) and for their assembly, on amyloidogenesis.

In the current work, we combined surface- and solution-sensitive techniques to investigate process of formation and growth of fibrils for a well-known peptide such as lysozyme (LYS) in the presence of polar and zwitterionic phospholipid molecules at concentrations below and above their critical micellar concentration (CMC), i.e., for solution containing only free lipid molecules (below 1 CMC), and a mixture of free molecules and lamellar aggregates (at and above 1 CMC). Our results show that, already at a concentration of 1 CMC, the presence of charged or zwitterionic lipid species free in solution augments the fibrils growth rate, with no clear differences for higher concentration values and no evident differences in mature fibrils structure. Moreover, we have monitored the interaction of native LYS, LYS fibrils, and LYS–lipid aggregates with a model bilayer composed of 1-palmitoyl-2-oleoyl-sn-glycero-3-phosphocholine (POPC), a zwitterionic phospholipid largely abundant in mammalian cell membranes. From these experiments, a clear trend shows that the affinity of aggregates for the POPC membrane is enhanced for LYS–lipid aggregates, while it is limited for LYS monomers and very small oligomers.

Materials and methods

Materials

Hen egg white lysozyme (LYS), glycine and Congo Red (CR) were purchased from Merck (Darmstadt, Germany). Phospholipids powders, POPC, and 1-palmitoyl-2-oleoyl-sn-glycero-3-phosphoglycerol (POPG) were purchased from Avanti Polar Lipids (Alabaster, USA).

CR is water soluble, but its solubility is better in organic solvents such as ethanol. We prepared an acqueous ethanol solution (80% w/w) saturated with NaCl. This solution was then saturated with CR powder and filtered with 0.2 μm pore size filters (Millipore) to remove possible aggregates. Lyophilized LYS was dissolved in glycine buffer (70 mM, pH 2.3 with 10 mM NaCl) at a concentration of 3 mg/mL. The buffer was previously filtered with 0.2 μm pore size filters (Millipore). The solution was maintained at 4°C overnight, according to already published protocols [23,24]. LYS amyloid fibrillation was induced at the temperature of 65°C [25] with gentle agitation to reach a plateau in the aggregation after about 2 h from the beginning of the fibrillation. LYS aggregation kinetics were monitored by taking quite small aliquots from a solution undergoing aggregation and measuring them as a function of the stage (time) of aggregation. In order to investigate the role of phospholipids in solution, as monomers or as vesicles, on the aggregation propensity of LYS, we used POPC and POPG. These lipids were dissolved in buffer at different concentrations, matching the nominal values of 0.25, 0.50, 1, 2, and 10 CMC. Dissolution was achieved by vortexing the samples. For samples at 1 and 10 CMC, the lipid solution was used in the extruded and non-extruded forms, where the latter was investigated just as prepared. For extruded samples, the solution was pushed 11 times through a polycarbonate filter having 100 nm pores. Extrusion was performed at room temperature. The size of the lipid aggregates was checked by dynamic light scattering (DLS). In the case of samples prepared at a concentration equal to 1 CMC, the scattered intensity was not sufficient to quantify the particle size, while for samples prepared at 10 CMC, DLS data indicated the formation of vesicles, very likely large uni-lamellar vesicles (LUVs) for the extruded samples, and multi-lamellar ones for the non-extruded solutions.

In order to measure the effect of lipids on LYS aggregation from the early onset of the process, lipid solutions were added to LYS shortly before the start of each kinetic of aggregation. For these samples, LYS and lipid were prepared at the proper concentration to maintain the final concentration of 3 mg/mL of LYS for all samples.

UV-Visible (UV-Vis) spectrophotometry

UV-Vis spectrophotometry experiments performed in the presence of CR can be used to monitor protein aggregation into amyloid structures. CR has a high affinity for β-sheet conformations of fibrillated proteins [26,27], and it has been used as a diagnostic tool for amyloidogenesis for several decades. Amyloid aggregates stained with CR alkaline solutions assume, in fact, an intense red color under sunlight and show birefringence under polarized light [28,29]. CR interaction with β-sheet structures induces a shift of its absorption maximum from 490 to 540 nm. It has been recently demonstrated that CR bound to amyloid fibrils is oriented with the long axis oblique to the fibril, characterized by an angular deviation that permits the mutual interaction between the aromatic moieties of the next CR molecules. This arrangement provides a molecular basis to justify the cooperative association of CR molecules along the fibril axis in the fibrillar microenvironment, and the constrained conformational flexibility can be interpreted as the main contribution to the bathochromic shift of the maximal absorbance wavelength when CR is bound to amyloids [30]. UV-Vis experiments were performed using quartz cuvettes with a 10 mm optical path, filled with 50 µL of protein sample (pH ≃ 2.3), 50 µL of CR solution, and 400 µL of 70 mM glycine buffer – the same used for LYS amyloid aggregation – with NaOH addition until pH was ≈11.5. The amount of CR used was chosen from protocols published in literature [25].

DLS

DLS is a technique commonly used to measure the size distribution of colloidal particles in solution. In the present case, DLS was used to track the aggregation of LYS over time, both in the absence and presence of lipid molecules. Experiments were performed on a Malvern Zetasizer Pro instrument (Malvern Panalytical, UK) configured in backscattering geometry (scattering angle, θ = 173°) and using an incident wavelength λ = 633 nm, produced by a He–Ne laser. Samples were loaded into standard quartz cuvettes (10 mm optical path) and kept at 25°C for the entire duration of the measurements. Aggregation kinetics were followed during a period of 6 h, acquiring data every 30 min in five replicas to ensure the reliability and reproducibility of the data. Single measurements, used to check the size of POPC vesicles, were performed in three replicas. All samples resulted in diluted regime, and no attenuation of the incident light was necessary. The intensity auto-correlation function $g_2(\tau) - 1$ was computed automatically by the instrument, where τ is the correlation constant. Intensity-weighted particle radius distribution was obtained by analyzing the $g_2(\tau) - 1$ data using a homemade software application (DynaLiSc) written in Matlab and based on the regularized inverse laplace transform method [31]. This method, is suitable for samples showing the coexistence of polydisperse particle populations, as typically occurring during aggregation processes. The conversion between results in the time domain to particle hydrodynamic radius was performed using the Stokes–Einstein equation:

$$R_{\mathrm{H}} = \frac{k_{\mathrm{B}}T}{6\pi\eta(T)D}, \tag{1}$$

where R_{H} is the hydrodynamic particle radius, k_{B} is the Boltzmann constant, T is the absolute temperature, $\eta(T)$ is the dynamic viscosity of the solution, and D is the particles' translational diffusion coefficient. The latter can be obtained from the characteristic decay time t^* of the auto-correlation function as $D = (t^*q^2)^{-1}$, where $q = \frac{4\pi n \sin(\theta/2)}{\lambda}$ is the scattering vector and n is the solution refractive index for the given λ. When using DLS, it is important to be aware that the scattered intensity from a few large particles may overwhelm that of smaller particles, leading to an underestimation of this second contribution. In extreme cases, as in the terminal stages of an unlimited growth of aggregates, this can even result in the complete masking of small particles by the signal from larger ones. Conversion to number-weighted size distributions was not performed deliberately, as the conversion method gives reliable results only for optically homogeneous spherical particles.

Quartz crystal microbalance (QCM)

QCM is a technique widely used to monitor adsorption processes at solid interfaces [32]. Briefly, this technique measures the frequency of vibration of a quartz crystal subject to an alternating potential. Changes in this frequency (ΔF) can be related to changes in the mass deposited on the sensor surface. Supported lipid bilayers (SLBs) deposited on silica-coated QCM sensors typically behave as thin rigid films, i.e., they oscillate in phase with the sensor

without dissipating mechanical energy. In this case, the Sauerbrey equation can be used to evaluate changes in adsorbed mass per unit area, Δm, as follows [33,34]:

$$\Delta m = -C_f \frac{\Delta F_n}{n}, \quad (2)$$

where C_f is the mass sensitivity constant (C_f = 4.4 ng Hz^{-1} cm^{-2} for an AT-cut quartz crystal with 10 MHz fundamental frequency) and n is the overtone number (n = 1 was utilized in the current work). Here, the QCM technique was used to investigate the interfacial behavior of LYS prepared at different stages of fibrillation in the presence of already formed SLBs. Measurements were performed both in the absence and in the presence of lipids co-dissolved with LYS in solution. QCM experiments were performed only on POPC samples since there are no established protocols for the formation of fully covered POPG SLBs. Indeed, incomplete coverage of the bilayer would compromise the investigation of LYS adsorption processes, as the peptide could interact with exposed areas on the silicon substrate used as substrate. Measurements were performed using an OpenQCM Q^{-1} equipment (Novaetech Srl, Italy) and SiO_2-coated AT-cut 10 MHz quartz sensors (Novaetech) at room temperature (23 ± 2°C). Before usage, the sensors were cleaned by 15 min bath sonication in ethanol. To remove any remaining contaminants and make the SiO_2 surface hydrophilic, the sensors were exposed for 30 min to UV-generated ozone (Jetlight model 18; Jelight, Irvine, USA). Finally, the surfaces were rinsed with MilliQ-grade water and blow dried using a nitrogen stream. The dry sensor was then placed in the sample chamber. Before measurements, the sample chamber was filled with 250 mM NaCl solution using a peristaltic pump (KF Technology, IT) at a flow rate of 0.1 mL/min until a stable baseline was obtained. SLBs were deposited on top of silica-coated sensors exploiting the vesicle fusion protocol [35,36]. POPC vesicles dispersed in pure water at a concentration of 0.5 mg/mL were injected into the sample chamber at a flow rate of 0.2 mL/min (for a total volume of 500 µL) and left to incubate for 10 min. As the sample chamber was pre-filled with 250 mM NaCl solution, water was used as solvent for the POPC LUVs to induce an osmotic shock promoting the fusion of the vesicles. Once the bilayer was formed, un-fused vesicles were removed by rinsing the sample with pure water. The frequency shift obtained was used to determine if a homogeneous and defect-free SLB formed (expected $\Delta F_1 \approx 100$ Hz on a 10 MHz sensor [37]). After the quality of the SLB was checked, water was replaced by buffer to acquire the correct baseline for the following peptide injections. Finally, peptide-containing solutions were injected into the cell and incubated for 2 h. During all of the steps, data were collected continuously.

Atomic force microscopy (AFM)

AFM measurements were performed on an AIST-NT scanning probe microscope (Horiba Scientific, Kyoto, Japan). Images were acquired in non-contact mode with a pyramidal silicon tip of radius of 8 nm. Samples were prepared from the batches that reached the end point of fibrillation and diluting them from the original concentration by a factor 1:1,000. The dilution factor was optimized empirically to avoid the deposition of more than one layer of peptides onto the mica surface. Briefly, 5 µL of the diluted solution were deposited onto freshly cleaved mica and left to incubate for 20 min. After incubation, the mica surface was rinsed with milli-Q water and dried with nitrogen blowdown. All images were acquired with a resolution of 512 × 512 pixels with a scan rate of 1 Hz and were analyzed with the Gwyddion software. For each sample, at least five images were acquired and analyzed.

Results and discussion

LYS amyloid aggregation was first monitored by UV–Vis spectrophotometry with CR. LYS is a model protein whose amyloidogenesis in the presence of osmolites had already been studied by the same approach [24,25]. The sigmoidal behavior of the growth of fibrils, which results from the red shift of CR absorption peak, is related to a kinetic process that can be compared to the one revealed by adding Thioflavin T to the protein solution and measuring fluorescence emission [38]. The sigmoidal growth of the signal can be quantitatively evaluated, and in particular, the time needed to reach the first half of the process can be obtained. The halftime can be considered as a measure of mutational effects on nucleation. As previously suggested, primary nucleation is not the only microscopic process during the lag time of aggregation [39]. Fibril-catalyzed secondary nucleation has been observed for the aggregation of $A\beta_{42}$ [10], $A\beta_{40}$ [40], and α-synuclein [41]. Whereas primary nucleation is the most active at the beginning of the lag phase, secondary nucleation would soon dominate and reach its maximal rate near the halftime of aggregation. Therefore, halftime can be considered an indicator for the overall nucleation rate when both primary and secondary nucleation reactions are present [42]. CR UV–Vis spectrophotometry experiments are based on the absorbance peak shift induced by CR binding to β-sheet structures, as shown in Figure 1(a). The ratio Abs_{538}/Abs_{505} between the absorbance at 538 nm and the one at 505 nm is proportional to the

amount of β structures in solution and is plotted as a function of time, in Figure 1(b) for LYS without any cosolutes and for LYS with non-extruded POPG molecules at a concentration equal to 1 CMC. The sigmoidal behavior of the growth of β-structures of LYS in solution resembles quite well the one revealed by ThT fluorescence in a previous study [25], and was fitted in order to obtain the halftimes, which determine each aggregation pattern. A histogram of the obtained halftimes for the investigated conditions is reported in Figure 2. We underline that every experimental condition refers to at least three replicas of protein aggregation kinetics. Although kinetic patterns at intermediate phospholipids concentrations (between 0.0 and 1.0 CMC) were investigated, they are not reported here because their features were well inside the limit cases, but their reproducibility did not allow us to infer a possible linearity of their contribution. On the other side, at phospholipids concentration higher than 1 CMC (10 CMC), the amyloid aggregation was very fast and less reproducible. The presence of phospholipids appeared to be a factor favouring the formation of aggregates. In particular, for both POPC and POPG at any of the investigated concentrations, CR UV–Vis measurements revealed that: (i) the amount of β-structures after 2 h from the triggering of the amyloidogenesis, represented by the ratio Abs_{538}/Abs_{505}, increased in the presence of lipids; (ii) lipids favor aggregation, since the halftime of the process is reduced in their presence, and (iii) the difference between the changes induced by the two lipids is not always so relevant. In addition, POPC effects on the halftime of the process are remarkably different if it is in LUVs or if it is not extruded (Figure 2). POPC has a CMC on the order of

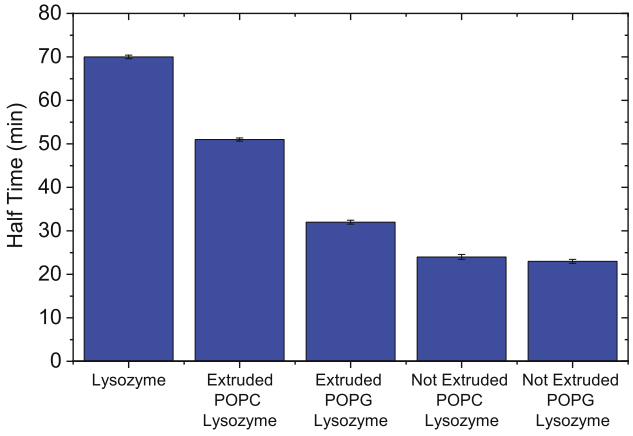

Figure 2: UV/Vis spectroscopy results on the effect of POPC and POPG, both at a concentration equal to 1 CMC, on lysozyme aggregation pattern. Histograms show the halftime obtained from the theoretical fitting of each aggregation pattern.

the nanomolar scale, while it can be noted that the oxidation products of POPC have CMC values on the order of the micromolar scale [43]. These changes in the CMC values could suggest that the susceptibility of model membranes composed of low-CMC phospholipids should increase in the presence of oxidatively damaged lipids due to their higher CMC promoting membrane insertion of amyloidogenic proteins and leading to formation of ion-channel-like pores [22]. The difference in the halftime of the process could hence reside in the fact that free lipids can form stable peptide–lipid complexes with LYS hydrophobic surfaces and then modify the protein aggregation rate in a quite different way in

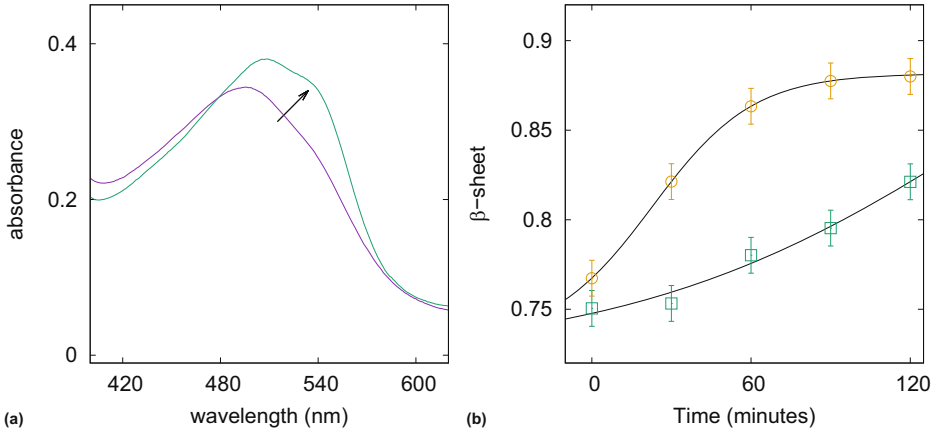

Figure 1: (a) UV-Vis spectroscopy results of lysozyme in solution in the presence of CR at the beginning (violet) and the end (green) of its aggregation pattern in the presence of POPG at 1 CMC, not extruded. The arrow indicates how the absorbance peak of CR shifts at higher wavelength when bound to β sheet structures. To monitor the relative amount of β-sheet structures in solution, the ratio between the intensity of the absorption peak due to CR bound to fibrils and the one due to CR free in solution was calculated as a function of time. (b) β-sheet structures as a function of time, during fibrillation. Empty squares correspond to lysozyme in solution without any cosolutes, and empty circles correspond to to lysozyme with non-extruded POPG molecules at a concentration equal to 1 CMC. Continuous lines are the theoretical fitting curves, providing the halftime featuring each kinetic pattern.

respect to the LUVs in solution. Further investigation concerning proteins with meaningfully different hydrophobic areas can help to confirm or discredit this hypothesis.

The aggregation of LYS in solution and in the presence and absence of different phospholipid molecules, before and after extrusion, was also evaluated by DLS. These experiments were conducted on arrested states of aggregation kinetics, i.e., by taking 1 mL aliquots from the stock solution at regular time intervals and measuring them after their temperature was lowered to 25°C to stop aggregation. In Figure 3, left panel, the intensity auto-correlation curves measured for LYS solutions in the absence of lipid molecules are reported. From the changes in the shape of the measured auto-correlation function, it is clear that a population of aggregates emerges, and increases in terms of amount, during the fibrillation process. Indeed, the data analysis revealed the coexistence, in all samples, of two populations of particles. At t = 0 s, the majority of the signal arises from *small* particles (with $R_H \approx 2.5 \pm 0.5$ nm) with a limited contribution from larger particles, with $R_H \approx 35 \pm 10$ nm (see black line in Figure 3, right panel). During the progression of the aggregation process, the predominant population remains the small one, with a size that is constant. On the other hand, a population of large aggregates, with radius ranging between 130 and 300 nm emerges. The area under the curve ascribed to this population increases with time, indicating an increase in the number of aggregates. The continuous growth of this population and the small shift towards larger radii indicate that the protein aggregation process is underway. Even if it is not possible to determine the true size of the aggregates (due to the approximations used in the standard DLS analyzis), these data clearly demonstrate, in line with UV–Vis (Figure 1(b)) and AFM (Figure 4) measurements, the occurrence of the aggregation kinetics and its timescale for the conditions used in our fibrillation protocol. When considering the amount of aggregates in solution, it is worth recalling that, because of the sensitivity of DLS, the vast majority of proteins in solution for all samples are in the range 2–3 nm, values compatible with the expected size for LYS monomers and small oligomers in solution [44]. However, even if it is not possible to discriminate between monomers and oligomers, we can hypothesized that during the process the balance between monomers and small oligomers changes as suggested by the increase of the β structures detected in UV–Vis experiments (Figure 1(b)). Such an increase indicates that protein native conformation is not maintained and that aggregation follows a path from monomers into dimers, then into oligomers, and finally into fibrils. For the LYS sample incubated with POPC and POPG molecules at 1 CMC, DLS measurements revealed a faster aggregation (Figures 5 and Figures S1, S2, S3 in the Supplementary material), in agreement with UV–Vis spectroscopy results (Figure 2). Given the expected limited number of lipid aggregates at 1 CMC, lipid molecules did not contribute substantially to the scattered intensity as determined by reference DLS measurements performed in the absence of peptides. The only signature of lipid aggregates was found for the LYS+POPC LUVs sample measured at time zero, as indicated by the shoulder in the intermediate time region of the $g_2(\tau) - 1$, corresponding to an LUV size in the range of 100–200 nm (Figure S1 in the Supplementary material).

Kinetics of aggregation were monitored for a total of 2 h in the case of POPC and 1 h in the case of POPG, both in extruded and non-extruded forms. Intensity auto-correlation functions and the size distributions resulting from their

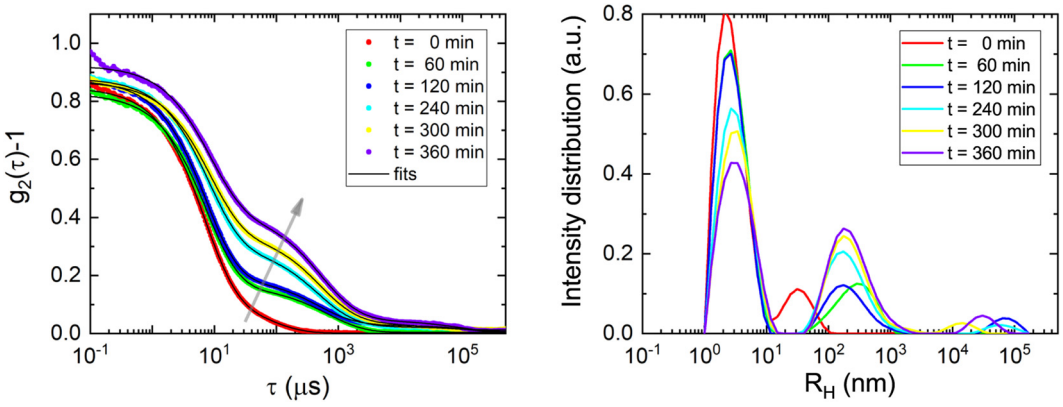

Figure 3: Left: intensity auto-correlation functions ($g_2(\tau)$ 1, symbols) for lysozyme solutions. Data were acquired at 60 minutes intervals from the beginning of the aggregation process. The arrow indicates the increase of aggregates contribution with time. Red lines are the model curves obtained from the analyzis. The increase in the experimental data visible at short times for some curves is an instrumental artifact. Right: intensity-weighted distributions of the hydrodynamic radius, R_H, corresponding to the model curves shown in the left panel.

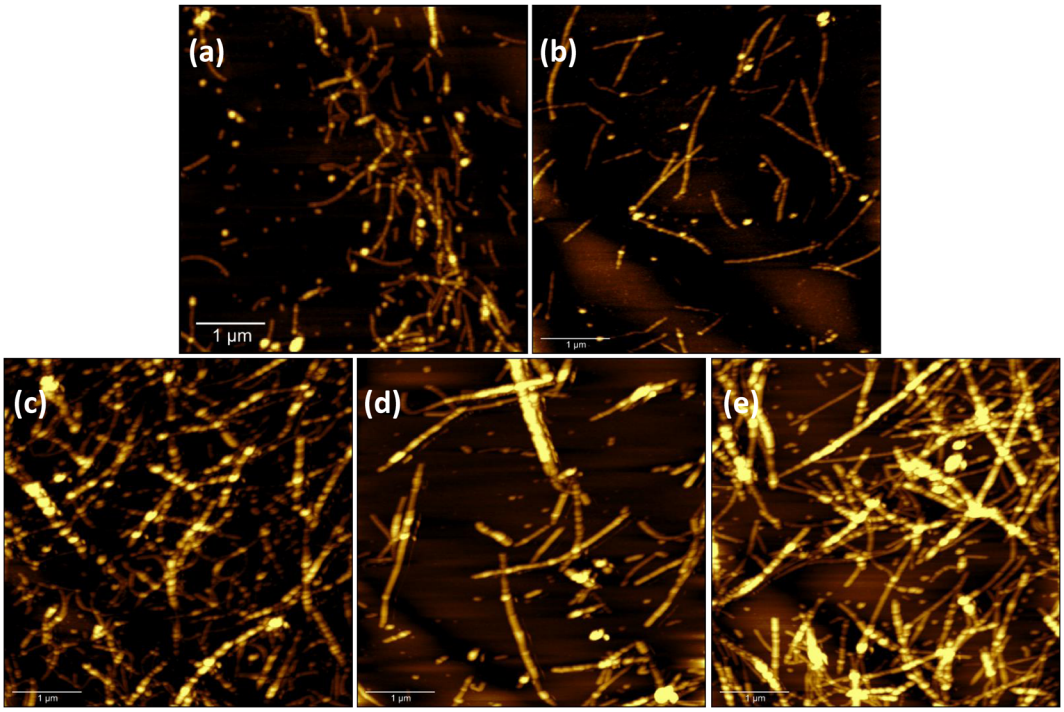

Figure 4: AFM images for (a) LYS, (b) LYS + POPG at 25% CMC, not-extruded, (c) LYS + POPG at 50% CMC, not-extruded, (d) LYS + POPG 1 CMC, not-extruded, and (e) LYS + POPG 1 CMC, extruded . Scale bar is 1 µm. The presence of fibrillar aggregates is visible for all samples. Their height increases slightly in the presence of lipid molecules, with no differences between zwitterionic and charged species.

analyzis are shown in Figures 5 and S1 for POPC and in Figures S2 and S3 for POPG. In all samples, the signal previously ascribed to LYS monomers and small oligomers was present. However, the contribution of this population was reduced to less than 50% of the total scattered intensity in the first 30 min for non-extruded POPC and almost disappeared in the presence of non-extruded POPG. In turn, the growth of a population of aggregates with $R_H \approx 110 \pm 20$ nm was observed in both cases. DLS measurements also allowed us to detect the presence of very limited amount, considered negligible, of larger aggregates ($R_H > 1$ µm). At the end of the aggregation process, the main contribution to the scattering intensity (≈ 80%) came, for both samples, from the aggregates population.

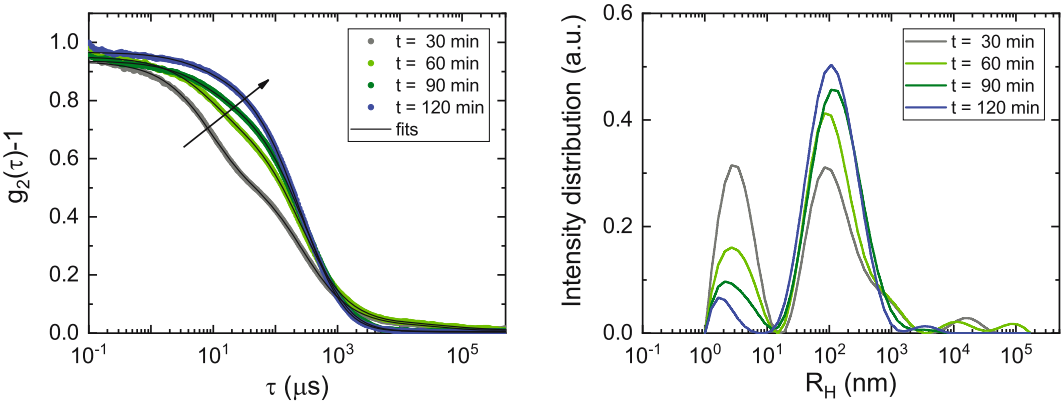

Figure 5: Left: Intensity auto-correlation functions (symbols) for lysozyme in the presence of non-extruded POPC molecules at a concentration equal to 1 CMC. Data were acquired at 30 minutes intervals from the beginning of the aggregation process. The arrow indicates the major changes in the correlation curves taking place with time. Red lines are the model curves obtained from the analyzis. The increase in the experimental data visible at short times for some curves is an instrumental artifact. Right: Intensity-weighted distributions of the hydrodynamic radius, R_H, corresponding to the model curves shown in the left panel.

A very similar trend was observed in the presence of POPC and POPG LUVs (Figures S1 and S3 in the Supplementary material). This was not unexpected as, at such concentration, the majority of lipid molecules are present in solution as monomers. The absence of noticeable differences in the DLS data measured with and without extruding the lipid solutions confirms the UV–Vis observations previously described. We underline that in all cases, the main changes were observed in the amount of LYS molecules contributing to different particle populations, while the size of these populations did not change appreciably during the aggregation processes.

In order to determine the morphology of the aggregates present in solution at the end of the aggregation process, we used AFM. AFM images for a set of the investigated samples are shown in Figure 4. The presence of amyloid fibrils, with typical length on the order of microns, is evident for all the samples. Their height, as well as of their width, resulted to be of a few nanometers, as in previous investigation on similar samples [24,45]. As the determination of the lateral size of particles with AFM is limited by tip-induced effects, we limited the quantitative analysis to the height determination. The latter was determined by sampling at least 50 aggregates per image, considering three images for each sample, and using the Gwyddions software. Their mean height values and the associated statistical error are shown in Figure 6 for the LYS and LYS + POPG samples, and in Figures S4 and S5 for LYS + POPC samples.

The presence of amyloid fibrils was revealed in all the samples, and no significant height differences were found between LYS + POPG and LYS + POPC samples.

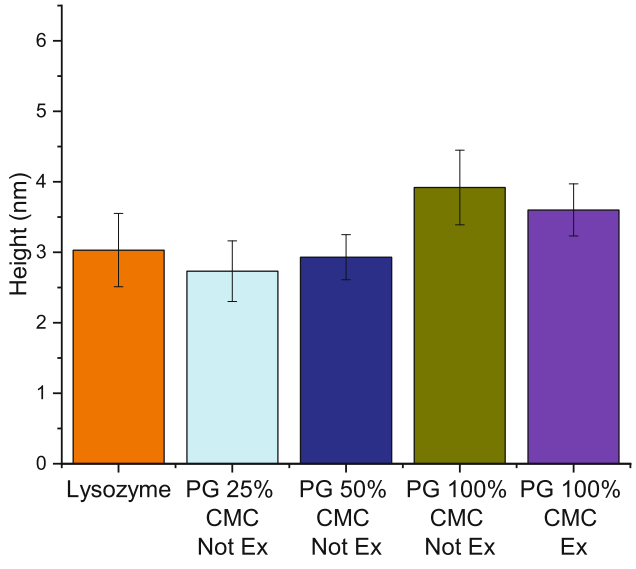

Figure 6: Mean value for fibrils height determined from AFM images.

UV–Vis spectroscopy and DLS experiments clearly indicated that the rate of aggregation is influenced by the presence of phospholipids in solution, even when their concentration is not sufficient to promote the formation of self-assembled structure, i.e., when it is lower than 1 CMC. LYS amyloid fibrils interaction with model membranes had been investigated, suggesting that fibrils induce reduction of bilayer hydration and increase of lipid packing in the interfacial region of model membranes [46]. However, at our knowledge no investigation has been performed on the influence of model membranes on LYS amyloid aggregation. On the other side, the influence of model membranes on peptides involved in severe diseases, like amyloid β peptide and α-synuclein, has been studied with conflicting results. Our results on LYS appear unequivocal and hence important to set a strategy to understand the pathway of interaction and of cytotoxicity for amyloid-forming peptides, as they can lead to cell depletion or membrane permeation.

In order to investigate the interaction of LYS, prepared at different stages of fibrillation alone and in the presence of lipid cosolutes, we performed QCM experiments using a POPC SLB as target model membrane. The SLB was deposited using the vesicle fusion method onto a silica-coated QCM sensor as described in the Materials and Methods section. The quality of the SLB was evaluated by measuring the frequency shift obtained after removal of any unfused vesicle and unbound lipid material. Afterwards, aliquots taken from the solution undergoing aggregation (containing either LYS or LYS + POPC) were injected in the sample cell using a peristaltic pump and left to incubate in stagnant flow condition. The interaction was monitored for 2 h. Finally, the process was stopped by rinsing the sample chamber with pure buffer to remove any unbound material and to evaluate the stability of the adsorbed layer.

The absolute frequency measured for the POPC SLB was taken as reference for the calculation of the frequency shifts (expected $\Delta F_1 \approx 100$ Hz on a 10 MHz sensor). In the case of the native LYS solution, QCM data showed the presence of a adsorption process with an average rate of 5.6 ng/cm^2 min^{-1} resulting in a final frequency shift $\Delta F_1 = -214 \pm 1$ Hz, corresponding to an adsorbed mass of 942 ± 4 ng/cm^2 (≈4 × 10^{13} LYS molecules on the 1 cm^2 sensor surface) (Figure 7). On the same sensor, there were originally ≈4 × 10^{14} POPC molecules as determined from the QCM data collected before incubation (not shown).

The presence of LYS aggregates in the solution promoted a faster interaction, as well as a larger adsorbed amount. Indeed, upon injection of the LYS aliquot taken 30 minutes after the onset of aggregation, the adsorption kinetics resulted faster (8.4 ng/cm^2 min^{-1}) as reported in

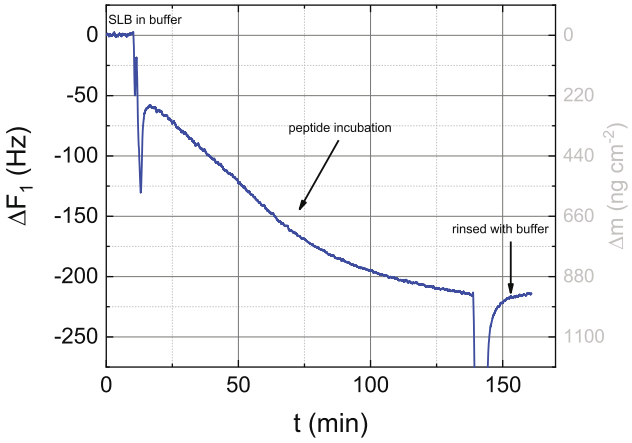

Figure 7: Changes of the 10 MHz frequency upon interaction between native lysozyme and a pre-formed POPC SLB. ΔF_1 = 0 Hz corresponds to a homogeneous POPC SLB adsorbed onto a silica-coated QCM sensor. On the right axis, the mass per unit area corresponding to the observed shift is indicated (equation (2)).

Figure 8, dashed line. The final adsorbed amount resulted almost double that in the case of native LYS (ΔF_1 = −418 ± 1 Hz, corresponding to Δm =1,840 ± 5 ng/cm^2 and to ≈7.8 × 10^{13} LYS molecules). In this case, the rinsing step, visible in the QCM trace at $t \approx 160$ minutes, stopped the adsorption before it reached equilibrium. In the presence of lipid co-solute, the rate of adsorption increased even more, reaching 25.4 ng/cm^2 min^{-1} for LYS + POPC at 1

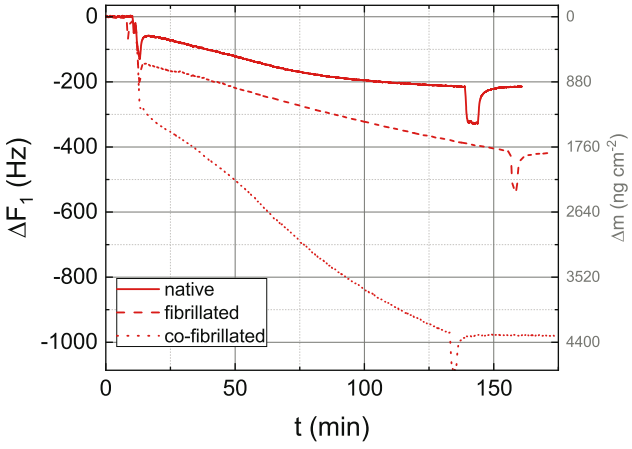

Figure 8: Frequency shifts (ΔF_1) measured by QCM for the 10 MHz frequency. The baseline (ΔF_1 = 0 Hz) corresponds to a homogeneous POPC SLB. For all samples, the interaction between this SLB and native LYS (solid line), aggregated LYS (dashed line), and LYS aggregated in the presence of POPC (1 CMC) was monitored for approx. 120 minutes. The interaction was stopped by washing off all unbound materials with pure buffer. Data were shifted along the time axis to overlap the solution injection point. On the right axis, the mass per unit area corresponding to the observed shift is indicated (equation (2)). Transient deeps in the frequency shifts are induced by the operation of the peristaltic pump.

CMC (dotted trace in Figure 8). In this case, the adsorption was stopped as the adsorbed mass was getting closer to the maximum load measurable by the instrument in the chosen configuration. After rinsing, the frequency stabilized at ΔF_1 = −978 ± 2 Hz (corresponding to $\Delta m \approx$ 4,300 ng/cm^2). In all three cases investigated, despite the large differences in adsorption rate and amount, the sample resulted to be stable upon rinsing, indicating no measurable desorption of material from the surface.

The QCM results, supported by the evidence provided by UV–Vis and DLS indicating the increased presence of aggregates in the LYS + lipids samples, suggest that aggregates are more prone to interact with a zwitterionic model membrane causing accumulation of material in its proximity. Upon interaction, aggregates are bound to the membrane as they are not removed during the rinsing steps applied. However, with the techniques used, it is not possible to determine their location and the structure and morphology of the final lipid–LYS film. As adsorption resulted to be enhanced for aggregates and as the solution flows on the top of the QCM sensor, a partial contribution of sedimentation cannot be excluded *a priori*. This hypothesis can be confuted on the basis of the DLS and AFM data, which indicate that the size of the aggregates was similar for all investigated samples. Sedimentation depends on the size of the particles, and therefore, the different rates of adsorption observed in QCM experiments cannot be simply originated by this phenomenon. Moreover, sedimentation for the native LYS solution (containing mostly monomers and small oligomers) is negligible in the 2-h time-window probed during QCM experiments. Finally, in none of the transparent vials containing the solutions having reached the final stage of aggregation was noted any sediment.

Conclusion

In conclusion, the current data showed that the presence of phospholipids appeared to be a factor favoring the formation of amyloid aggregates. Indeed, UV–Vis spectrophotometry data revealed that the amount of -structures after 2 h from the triggering of the amyloidogenesis, increased in presence of POPG and POPC at different concentrations with a faster fibrillation rate of LYS in presence of these two lipids. The presence of POPG and POPC resulted in a remarkable reduction of the halftime of the nucleation process for samples containing these lipids. The presence of POPG and POPC does not alter the main structural features of fibrils, as revealed by AFM, and the difference between the changes induced by the two lipids in terms

of kinetic is not so relevant. DLS data confirmed spectrophotometry results by showing the existence of two main populations corresponding to small particles with $R_H \approx 2.5 \pm 0.5$ nm and large particles with radius ranging between 130 and 300 nm in all samples. Scattering contribution of these populations changes during the process in accordance with the formation of aggregates. LYS samples incubated with POPC and POPG molecules at 1 CMC showed a faster aggregation and the presence of another population of aggregates with $R_H \approx 110 \pm 20$ nm. The dimension of this range is compatible with the presence of aggregates and LUVs for samples containing extruded lipids. AFM images showed the presence of fibrils in all samples, with typical lengths on the order of microns, but with no significant height differences among samples. Finally, QCM data showed a decrement of the weight ratio between POPC and LYS for samples containing LYS fibrils compared with those with native protein, demonstrating that amyloid aggregates have a higher interaction with POPC SLB compared with the native one. All these results confirm an enhancing role of lipids on amyloid fibrillation as already shown in a recent work [47] and show a probable interaction mechanism of fibrils with model membrane. This interactions are consistent with the "lipid-chaperon hypothesis" [22]. According to this hypothesis, the interaction mechanism of amyloid fibrils with membranes, and the connected damage, is different depending on the peculiar CMC of interacting lipids. In particular, lipids with higher CMC suppress fibrils formation promoting pores formation into membranes. On the other side lipids with a lower CMC enhance a "detergent-like" mechanism of the amyloid fibrils causing lipids leakage and membranes damage. Since our work is limited to a model protein, it cannot suggest noticeable consequences on the interaction between peptides leading to amyloid fibrils and model membrane, adding hypothesis on neurological damages. However, our work demonstrates that methodological studies that include different biophysical techniques can provide important information on the influence of model membrane, with different features, on amyloid aggregation.

Acknowledgments: All authors acknowledge the Department of Life and Environmental Science (DISVA) in Marche Polytechnic University (UNIVPM) for providing access to the DLS instrument acquired within the project for Excellence Departments funded by MIUR (art. 1, comma 314-338, D Lgs 232, 2016).

Funding information: MGO thanks for the economic support provided by the European Union-Next Generation EU, Project Code: ECS00000041, Project Title: Innovation, digitalization and sustainability for the diffused economy in Central Italy-VITALITY. YG acknowledges the support by the "Fondo di Solidarietá Scientifica" awarded by the DISVA department (UNIVPM) for the purchase and commissioning of the QCM apparatus.

Conflict of interest: Authors state no conflict of interest.

Data availability statement: The datasets generated during and/or analysed during the current study are available from the corresponding author on reasonable request.

References

[1] Chiti F, Dobson CM. Protein misfolding, functional amyloid, and human disease. Annu Rev Biochem. 2006;75:333–66.

[2] Nelson R, Sawaya MR, Balbirnie M, Madsen AO, Riekel C, Grothe R, et al. Structure of the cross-beta spine of amyloid fibrils. Nature. 2005;435:773–8.

[3] Langkilde AE, Vestergaard B. Methods for structural characterization of prefibrillar intermediates and amyloid fibrils. FEBS Letters. 2009;583(16):2600–9. doi: 10.1016/j.febslet.2009.05.040.

[4] Goldschmidt L, Teng PK, Riek R, Eisenberg D. Identifying the amylome, proteins capable of forming amyloid-like fibrils. Proc Nat Acad Sci. 2010;107(8):3487–92.

[5] Cao Y, Mezzenga R. Food protein amyloid fibrils: Origin, structure, formation, characterization, applications and health implications. Adv Colloid Interface Sci. 2019;269:334–56. https://www.sciencedirect.com/science/article/pii/S0001868619301058.

[6] Martorana V, Raccosta S, Giacomazza D, Ditta LA, Noto R, Biagio PLS, et al. Amyloid jams: mechanical and dynamical properties of an amyloid fibrillar network. Biophys Chemistry. 2019;253:106231. https://www.sciencedirect.com/science/article/pii/S030146221930290X.

[7] Iadanza MG, Jackson MP, Hewitt EW, Ranson NA, Radford SE. A new era for understanding amyloid structures and disease. Nature Rev Mol Cell Biol. 2018;19:755–73.

[8] Glabe CG, Kayed R. Common structure and toxic function of amyloid oligomers implies a common mechanism of pathogenesis. Neurology. 2006;66 (1 suppl 1):S74–8. https://n.neurology.org/content/66/1_suppl_1/S74.

[9] Lorenzen N, Nielsen SB, Yoshimura Y, Vad BS, Andersen CB, Betzer C, et al. How epigallocatechin gallate can inhibit α-synuclein oligomer toxicity in vitro. J Biol Chem. 2014;289(31):21299–310.

[10] Cohen SIA, Linse S, Luheshi LM, Hellstrand E, White DA, Rajah L, et al. Proliferation of amyloid-β 42 aggregates occurs through a secondary nucleation mechanism. Proc Nat Acad Sci. 2013;110(24):9758–63. doi: 10.1073/pnas.1218402110.

[11] Oropesa-Nunnnez R, Seghezza S, Dante S, Diaspro A, Cascella R, Cecchi C, et al. Interaction of toxic and non-toxic HypF-N oligomers with lipid bilayers investigated at high resolution with atomic force microscopy. Oncotarget. 2016;7(29):44991–5004. http://www.oncotarget.com/fulltext/10449.

[12] Malmo C, Vilasi S, Iannuzzi C, Tacchi S, Cametti C, Irace G, et al. Tetracycline inhibits W7FW14F apomyoglobin fibril extension and keeps the amyloid protein in a pre-fibrillar, highly cytotoxic state. FASEB J. 2006;20:346–7.

[13] Iacono D, Markesbery WR, Gross M, Pletnikova O, Rudow G, Zandi P, et al. The Nun study. Neurology. 2009;73(9):665–73. https://n.neurology.org/content/73/9/665.
[14] Broersen K, Rousseau F, Schymkowitz J. The culprit behind amyloid beta peptide related neurotoxicity in Alzheimer's disease: oligomer size or conformation? Alzheimers Res Ther. 2010;2(4):12. http://www.ncbi.nlm.nih.gov/pubmed/20642866.
[15] Martel A, Antony L, Gerelli Y, Porcar L, Fluitt A, Hoffmann K, et al. Membrane permeation versus amyloidogenicity: a multitechnique study of Islet amyloid polypeptide interaction with model membranes. J Amer Chem Soc. 2017;139(1):137–48.
[16] Bacon H, Toppozini L, Rheinstädter M.. The interaction between amyloid-β peptides and anionic lipid membranes containing cholesterol and melatonin. PLoS One. 2014 June;9:e99124.
[17] Hane F, Drolle E, Gaikwad R, Faught E, Leonenko Z. Amyloid-beta aggregation on model lipid membranes: an atomic force microscopy study. J Alzheimers Dis. 2011 June;26:485–94.
[18] Sanderson JM. The association of lipids with amyloid fibrils. J Biol Chem. 2022 Aug;298(8):102108.
[19] Dubackic M, Linse S, Sparr E, Olsson U. Comparing α-synuclein fibrils formed in the absence and presence of a model lipid membrane: a small and wide-angle X-ray scattering study. Front Soft. Matter. 2022;1:741996. https://www.frontiersin.org/articles/10.3389/frsfm.2021.741996.
[20] Lindberg DJ, Wenger A, Sundin E, Wesén E, Westerlund F, Esbjörner EK. Binding of Thioflavin-T to amyloid fibrils leads to fluorescence self-quenching and fibril compaction. Biochemistry. 2017;56(16):2170–4.
[21] Scollo F, Tempra C, Lolicato F, Sciacca MFM, Raudino A, Milardi D, et al. Phospholipids critical micellar concentrations trigger different mechanisms of intrinsically disordered proteins interaction with model membranes. J Phys Chem Lett. 2018 Aug;9(17):5125–9.
[22] Sciacca MF, Lolicato F, Tempra C, Scollo F, Sahoo BR, Watson MD, et al. Lipid-chaperone hypothesis: a common molecular mechanism of membrane disruption by intrinsically disordered proteins. ACS Chem Neurosci. 2020 Dec;11(24):4336–50.
[23] Poniková S, Antošová A, Demjén E, Sedláková D, Marek J, Varhač R, et al. Lysozyme stability and amyloid fibrillization dependence on Hofmeister anions in acidic pH. J Biol Inorganic Chem. 2015;20(6):921–33.
[24] Mastrella L, Moretti P, Pieraccini S, Magi S, Piccirillo S, Ortore MG. Taurine stabilizing effect on lysozyme. Life. 2022 Jan;12(1):133. doi: 10.3390/life12010133.
[25] Mari E, Ricci C, Pieraccini S, Spinozzi F, Mariani P, Ortore MG. Trehalose effect on the aggregation of model proteins into amyloid fibrils. Life. 2020;10(5):60. https://www.mdpi.com/2075-1729/10/5/60.
[26] Klunk WE, Jacob RF, Mason RP. Quantifying amyloid by congo red spectra shift assay. Methods Enzymol. 1999;309(1974):6879.
[27] Khurana R, Uversky VN, Nielsen L, Fink AL. Is congo red an amyloid-specific dye? J Biol Chem. 2001;276(25):22715–21.
[28] Nilsson MR. Techniques to study amyloid fibril formation in vitro. Methods. 2004;34(1):151–60.
[29] Howie AJ, Brewer DB. Optical properties of amyloid stained by Congo red: History and mechanisms. Micron. 2009;40(3):285–301. https://www.sciencedirect.com/science/article/pii/S0968432808002187.
[30] Espargar A, Llabró S, Saupe SJ, Curutchet C, Luque FJ, Sabaté R.. On the binding of congo red to amyloid fibrils. Angewandte Chemie Int Edition. 2020;59(21):8104–7. https://onlinelibrary.wiley.com/doi/abs/10.1002/anie.201916630.
[31] Marino IG. RILT; https://la.mathworks.com/matlabcentral/fileexchange/6523-rilt.
[32] Easley AD, Ma T, Eneh CI, Yun J, Thakur RM, Lutkenhaus JL. A practical guide to quartz crystal microbalance with dissipation monitoring of thin polymer films. J Polymer Sci. 2022;60(7):1090–107.
[33] Sauerbrey G. Verwendung von Schwingquarzen zur Wägung dü nner Schichten und zur Mikrowägung. Z Phys. 1959;155(2):206–22.
[34] Höök F. Development of a novel QCM technique for protein adsorption studies. Göteborg, Sweden: Chalmers University of Technology; 1997.
[35] Kalb E, Frey S, Tamm LK. Formation of supported planar bilayers by fusion of vesicles to supported phospholipid monolayers. Biochimica et Biophysica Acta (BBA) - Biomembranes. 1992;1103(2):307–16.
[36] Cremer PS, Boxer SG. Formation and spreading of lipid bilayers on planar glass supports. J Phys Chem B. 1999;103(13):2554–59.
[37] Montis C, Gerelli Y, Fragneto G, Nylander T, Baglioni P, Berti D. Nucleolipid bilayers: a quartz crystal microbalance and neutron reflectometry study. Colloids Surfaces B Biointerfaces. 2016;137:203–13.
[38] Holm NK, Jespersen SK, Thomassen LV, Wolff TY, Sehgal P, Thomsen LA, et al. Aggregation and fibrillation of bovine serum albumin. Biochimica et Biophysica Acta - Proteins and Proteomics. 2007;1774(9):1128–38.
[39] Arosio P, Knowles TPJ, Linse S. On the lag phase in amyloid fibril formation. Phys Chem Chem Phys. 2015;17:7606–18. doi: 10.1039/C4CP05563B.
[40] Meisl G, Yang X, Hellstrand E, Frohm B, Kirkegaard JB, Cohen SIA, et al. Differences in nucleation behavior underlie the contrasting aggregation kinetics of the Aβ 40 and Aβ 42 peptides. Proc Nat Acad Sci. 2014;111(26):9384–9. http://www.pnas.org/lookup/doi/10.1073/pnas.1401564111.
[41] Buell AK, Galvagnion C, Gaspar R, Sparr E, Vendruscolo M, Knowles TPJ, et al. Solution conditions determine the relative importance of nucleation and growth processes in α-synuclein aggregation. Proc Nat Acad Sci. 2014;111(21):7671–6. https://www.pnas.org/doi/abs/10.1073/pnas.1315346111.
[42] Hsu F, Park G, Guo Z. Key residues for the formation of Aβ 42 amyloid fibrils. ACS Omega. 2018;3(7):8401–7. PMID: 30087945. doi: https://doi.org/10.1021/acsomega.8b00887.
[43] Pande AH, Kar S, Tripathy RK. Oxidatively modified fatty acyl chain determines physicochemical properties of aggregates of oxidized phospholipids. Biochimica et Biophysica Acta (BBA) - Biomembranes. 2010;1798(3):442–52. https://www.sciencedirect.com/science/article/pii/S0005273610000039.
[44] García de la Torre J, Huertas ML, Carrasco B. Calculation of hydrodynamic properties of globular proteins from their atomic-level structure. Biophys J. 2000;78(2):719–30.
[45] Booth DR, Sunde M, Bellotti V, Robinson CV, Hutchinson WL, Fraser PE, et al. Instability, unfolding and aggregation of human lysozyme variants underlying amyloid fibrillogenesis. Nature. 1997;385:787–93. https://www.nature.com/articles/385787a0#article-info.
[46] Kastorna A, Trusova V, Gorbenko G, Kinnunen P. Membrane effects of lysozyme amyloid fibrils. Chem Phys Lipids. 2012;165(3):331–7. https://www.sciencedirect.com/science/article/pii/S0009308412000199.
[47] Rasmussen H, Otzen D, Pedersen J. Induction, inhibition, and incorporation: Different roles for anionic and zwitterionic lysolipids in the fibrillation of the functional amyloid FapC. J Biol Chem. 2022 Feb;298(2):101569.